Journal of Photochemistry & Photobiology, B: Biology 153 (2015) 296–304

Contents lists available at ScienceDirect

Journal of Photochemistry & Photobiology, B: Biology

journal homepage: www.elsevier.com/locate/jpb

Effect of photodamage on the outermost cuticle layer of human hair

M. Richena, C.A. Rezende *

Institute of Chemistry, University of Campinas — UNICAMP, P.O. Box 6154, 13084-971 Campinas, SP, Brazil

ARTICLE INFO

Article history:
Received 9 June 2015
Received in revised form 9 October 2015
Accepted 13 October 2015
Available online 22 October 2015

Keywords:
Human hair
Cuticle
Morphology
Photodamage

ABSTRACT

The surface of the hair is the region most exposed to solar radiation and to the environment in general. Many of the well-known damaging effects of sun exposure on hair must start or even be restricted to the most external cuticle layers. As such, this work investigates morphological, ultrastructural and chemical changes in the outermost cuticle layer of dark brown hair, using atomic force microscopy (AFM), field emission scanning electron microscopy (FESEM) and attenuated total reflectance Fourier transform infrared spectroscopy (ATR-FTIR). The results showed that after 230 h of irradiation with a mercury lamp, small bumps with globular shape (heights lying in the 1–5 nm range) appeared on the cuticle surface and their size increased with increasing irradiation times. In addition, the enlargement of pre-existing holes was also observed (holes increase around 350% in depth) and the height of the steps formed between the edges of two cuticle scales increased around 65%, as a result of 500 h of irradiation. The damages in hair strands were accurately identified by analyzing exactly the same surface region before and after irradiation by AFM images. Finally, the results were discussed in terms of the chemical differences between the non-irradiated and the irradiated hair, for instance, the increased level of cystine oxidation as a consequence of photodegradation.

1. Introduction

Changes in hair color due to sunlight exposure are a well-known effect in hair science [1,2,3]. Also, the damaging action of irradiation on hair chemical components, such as proteins, lipids and melanin pigments [4,5,6,7] has been reported. Hoting et al. [5] using amino acid analyses, showed that photodamaging is more pronounced in amino acid residues from the outermost layers of the hair strand than on those from the inner layers. These authors assigned this effect to the absence of melanin, which is the pigment responsible for photoprotection, in the outer hair layers. In a previous paper [1], we also showed that the photobehavior of white hair, irradiated with a mercury vapor lamp or with solar radiation, is dependent on the wavelength range of the incident radiation and on the initial shade of yellow in the sample.

Concerning the changes in hair morphology and ultrastructure due to photodegradation [8,9,10] there are only a few studies addressing this topic. Since the cuticle is the most external layer of the hair strand, it is the one most exposed to chemical and environmental damages. Cuticle cells are closely arranged forming 5 to 10 overlapping layers from the root towards the tip of the hair and provide a chemically resistant sheet protecting the internal hair components, such as the cortex and the medulla. The cuticle is formed by amorphous material and each cuticle cell is divided into four subunits that have a distinct chemical composition [11,12]: 1) The endocuticle, which is the most internal layer, is made up of non-keratinous material (≈3% *w*/*w* cystine) and is hydrophilic; 2) The exocuticle and 3) The A-layer are both hydrophobic and more reticulated, due to the higher cystine content (≈15% and ≈ 30% *w*/*w*, respectively); and 4) The epicuticle, which is the most external layer of the cuticle cell, and is thin (≈2.5 nm), hydrophobic and cystine-rich (≈12% *w*/*w*). The cystine groups of the epicuticle are bound to a lipidic layer (18-methylenicosanoic acid), forming a proteolipidic membrane that covers the cuticle [13]. The study of radiation effect on the cuticle is remarkably important, due to its protective role for the hair internal structures.

Weigmann et al. [8,9] used field emission scanning electron microscopy (FESEM) to analyze the UV radiation effect on hair surface and concluded that the cuticle is the region most affected by photodegradation, due to its high cystine concentration. They also observed that humidification cycles, intercalated with the UV irradiation periods, intensified the damages, since they caused thinning of the cuticle cell. The thinning of the surface cuticle was also observed by Longo et al. [10] that used scanning electron microscopy (SEM) and atomic force microscopy (AFM) to investigate the morphology of Caucasian black hair irradiated for 160 h with a xenon lamp. These samples were irradiated under high relative humidity and temperature (50–100% and 60 °C, respectively) and the most important photodegradation effects observed were the extraction of the cuticle scales and the formation of bubbles (≈200 nm) on the cuticle surface. Both papers studied the photodegradation action by comparing different strands in blended hair sample (mix of strands of many heads) [8,9,10].

It is a great challenge, however, to distinguish the photodamage effects on hair, because of the intrinsic morphological and chemical variations in hair strands. These differences can be found between strands

* Corresponding author. Tel.: +55 19 3521 3018.
E-mail address: marrichena@iqm.unicamp.br (C.A. Rezende).

http://dx.doi.org/10.1016/j.jphotobiol.2015.10.008
1011-1344/

from different heads (genetic variability), or between strands with distinct degradation levels from the same head or even between the root and the tip in a single hair strand. Dubief [14], for instance, showed a drastic increase in the cysteic acid content detected by infrared spectroscopic (IR) between the roots and the tip ends of virgin hair. This author suggests that this effect was caused by photo-oxidation, since cysteic acid is known to be a product of cystine photodegradation [15]. Also, Swift and Smith [16] showed that the hair surface is significantly changed along the hair length. While the scale edges present a smoother and more regular contour close to the strand root, as the distance increases towards the strand tip, the scale contour becomes more uneven, rougher and partially broken.

To overcome the intrinsic differences in hair strands before irradiation, it is important to obtain statistically representative images by analyzing: many strands from the same sample; and many different regions from each strand. The third interesting approach is to acquire images from the same region in the same sample before and after irradiation, so that the photodegradation effects on hair can be isolated from the pre-existing differences [17,18]. AFM is a very promising technique for such approach, because it is non-invasive and it does not require sample preparation (such as sputtering, carbon evaporation, microtome cutting or staining), allowing the samples to be analyzed in their natural state. Luengo and collaborators applied this methodology of analyzing the same sample area to investigate chemical properties of the human hair cuticle and its changes following a bleaching process. Chemically modified AFM tips, terminated with CH_3— and NH_2— groups, were used to achieve chemical contrast between hydrophobic and hydrophilic regions on the surface [18].

In the present work, the three approaches were used to investigate the photodegradation action on the morphology of hair cuticles. AFM is used to evaluate morphological changes taking place in exactly the same area on the sample surface before and after irradiation with a mercury lamp for periods up to 500 h. To our knowledge, this is the first time this methodology is applied with this purpose. Besides this, we used FESEM to scan different strands in each sample and different areas in the same strand, so that the results could be considered statistically valid. FESEM is a very convenient technique for sample mapping, because it allows a broad range of magnifications that can be easily and quickly adjusted during scanning. Finally, the chemical changes as a consequence of photodegradation were evaluated using attenuated total reflection (ATR).

2. Experimental

2.1. Samples

Dark brown hair was purchased from De Meo Brothers Inc. located in New York, USA (called “blended brown hair” along the text). Dark brown hair was also collected from one volunteer with no history of chemical treatments (called “brown hair from single-donor” along the text).

Prior to the experiments, the hair samples were washed with a 2.0% *w/w* sodium lauryl sulfate aqueous solution, according to the following steps: 1) hand-washing with 1 mL of the solution for 1 min; 2) rinsing with tap water at room temperature for 30 s; and 3) repetition of steps 1 and 2, but with rinsing for 2 min. The samples were then dried at room temperature and stored in plastic bags.

2.2. Radiation Sources

A mercury vapor lamp (OSRAM HQL 125 W, São Paulo, Brazil) was used as a radiation source. The lamp has an emission spectrum with UV (367 nm) and visible light (406, 438, 548 and 580 nm) intense lines (Fig. 1), in addition to emitting very low infrared (IR) radiation. It is thus very different from the continuous solar spectrum. The overall procedure for irradiation with a mercury vapor lamp is described elsewhere [3]. Measurements of light intensity from the source were carried out with a radiometer (PMA 2100, Solar Light Co., USA), considering the incident dose on the samples. The distances from the source to the sample and from the source to the radiometer were the same.

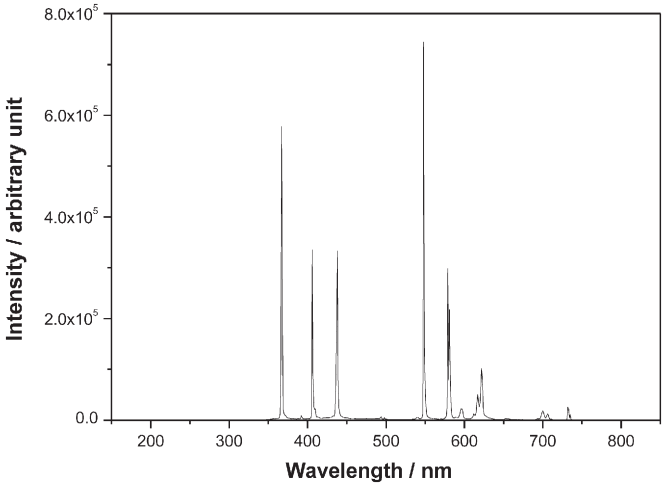

Fig. 1. Emission spectrum of the mercury vapor lamp (125 W).

2.3. Sample Irradiation

Hair strands were daily irradiated using a mercury lamp full-spectrum (UV, Vis and IR) for a 10 h period, which was followed by a 14 h period in the dark (inside a laboratory cabinet), after which the sequence was repeated cyclically. Irradiation was carried out inside a fume hood, as described elsewhere [3], for periods of 230, 500 or 600 h. The temperature and the relative humidity inside the fume hood were monitored daily and kept under 29.3 ± 0.9 °C and 44 ± 4% average values, respectively. The temperature data indicate that the mercury lamp emitted very low IR radiation. The doses of radiation intensity obtained for the mercury vapor lamp during the 10 h exposure were: 1.6 J cm^{-2} (UVB), 56.0 J cm^{-2} (UVA), 11.0 J cm^{-2} (Vis) and 313.0 J cm^{-2} (IR).

2.4. Atomic Force Microscopy (AFM)

AFM images were obtained in non-contact mode, using a Park NX10 Scanning Probe Microscope from the National Laboratory of Nanotechnology (LNNano/CNPEM), located in Campinas, SP, Brazil. The temperature was controlled at approximately 24 °C and the relative humidity was kept under 15% by a N_2 flow. Measurements were carried out using SiN_4 probes (NANOWORLD), NCHR model, with a 320 kHz nominal resonance frequency, a 42 N m^{-1} constant force and a typical tip diameter around 15 nm. Images with improved resolution were obtained with a sharper tip (SSSNCH model, with approximately 3 nm diameter). Blended hair strands were fixed on the sample holder by their ends, using silver adhesive. Images were obtained in three different strands of the sample (2 areas per strand, 10–60 images per strand). The same areas were imaged before and after irradiation. The software Gwyddion 2.36 was used for data treatment and to obtain the root mean square (RMS) roughness from topography images. RMS roughness is defined as the standard deviation of the height (z values) within the selected area (1 μm × 1 μm):

$$\mathrm{RMS} = \sqrt{\frac{\sum (Z_n - Z_{ave})^2}{N}} \quad (1)$$

where z_{ave} is the average of the z value within a specific area, z_n is the z value for a given point within this area and N is the number of measured points.

2.5. Field Emission Scanning Electron Microscopy (FESEM)

Secondary electron images (SEI) were obtained on the surface of hair samples using a high resolution environmental scanning electron microscope, equipped with a field emission gun (FEI, Quanta 650, USA). One centimeter long individual hair strands (3 strands/sample) were fixed on the sample holder stub and samples were coated with gold in a SCD 050 sputter coater (Oerlikon-Balzers, Balzers, Lichtenstein). Both the coater and the microscope were available at the National Laboratory of Nanotechnology (LNNano/CNPEM), in Campinas, SP, Brazil. Images were obtained under vacuum, using a 4 kV accelerating voltage and at least 10 images were obtained on different areas of each sample to ensure the reproducibility of the results.

2.6. Attenuated Total Reflectance Fourier Transform Infrared Spectroscopy (ATR-FTIR)

ATR-FTIR spectra data were obtained using an infrared microprobe for optical microscopy IlluminatIR II, Smiths, coupled to an Olympus BX51 optic microscope, with a fixed resolution of 4 cm^{-1}. Five hair strands were individually measured in their central areas before and after irradiation with the mercury lamp.

3. Results and Discussion

3.1. Topography Changes with Irradiation

Topography changes on the outer cuticle surface from dark brown hair due to irradiation were evaluated by AFM non-contact scanning mode. Fig. 1 shows two different strands (1 and 2), where the same surface area was imaged before (Fig. 2 (a) and (c)) and after irradiation with a mercury lamp for 500 h (Fig. 2 (b) and (d)). A relatively large area (15 × 60 μm) was scanned, allowing various scales to be observed at the same time, as shown in Fig. 2 (which was cut to a final 10 × 43 μm size). At this magnification, topography images obtained prior to irradiation or after it are very similar, showing a typical hair surface morphology, formed by superimposed scales, with a flat surface in general, although deposited residues and holes can be observed in some

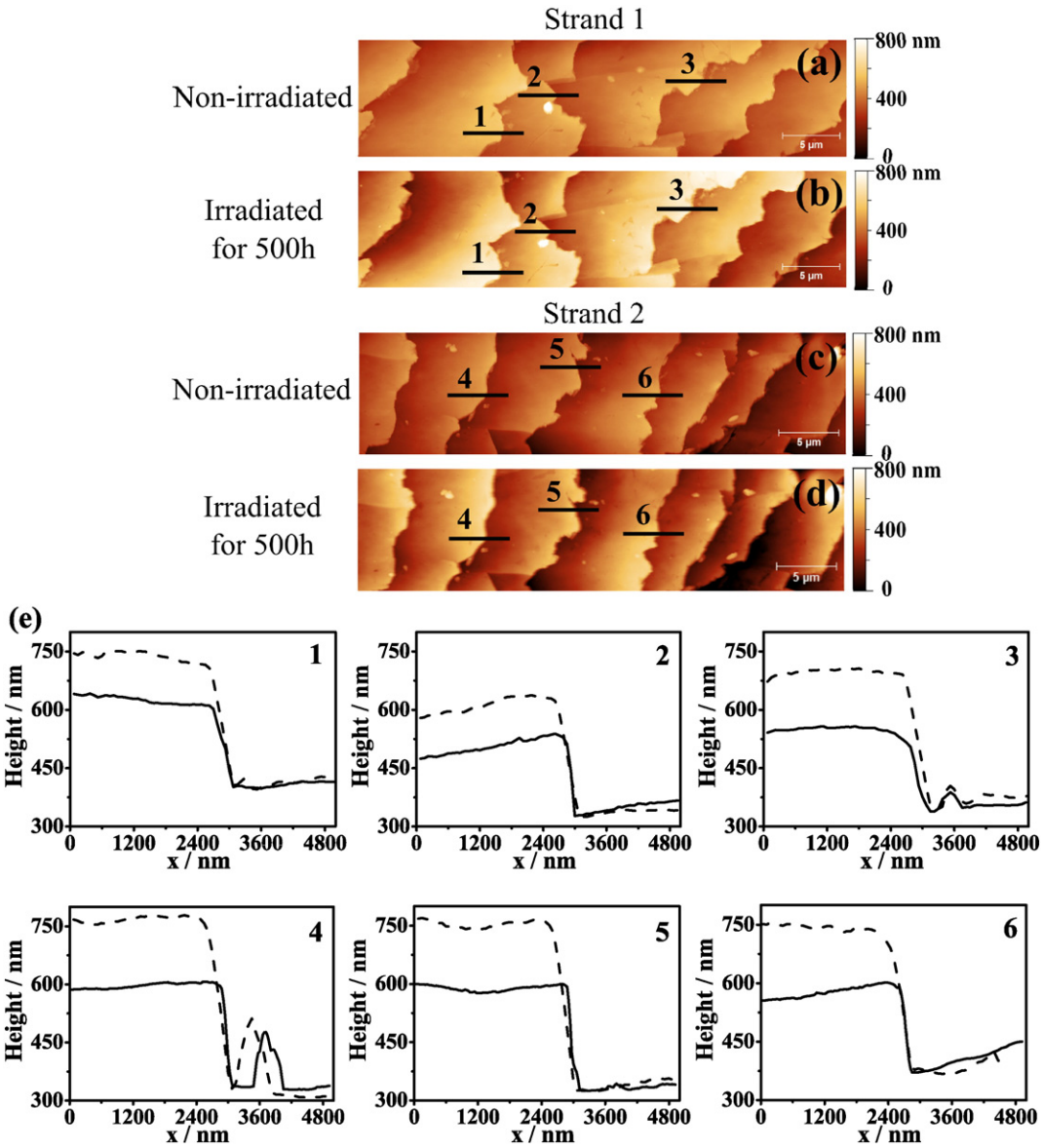

Fig. 2. AFM results obtained in two strands of blended dark brown hair before and after 500 h of irradiation with a mercury lamp: (a) Topography before and (b) after irradiation in the same area on strand 1; (c) Topography before and (d) after irradiation in the same area on strand 2; (e) Height profiles including the cuticle edge in positions indicated by the numbered lines in strands 1 and 2 before (—) and after (— — —) irradiation.

regions. The scale edges present an uneven contour, due to the detachment of small broken pieces.

To evaluate the possible height changes due to irradiation, height profiles were obtained from the AFM topography images in different regions on the cuticle scales, always including the edge. The positions of the line profiles (numbered from 1 to 6) are indicated in Fig. 2 (a–d), while the corresponding height profiles are shown in Fig. 2 (e). The same line was measured in strands 1 and 2 before and after irradiation and the images underwent the same leveling procedure so that the profiles could be compared. It is possible to observe that the height of the steps formed between the edges of two cuticle scales increased due to photodegradation (Fig. 2 (e)). The average step height for non-irradiated hair strands was 203 ± 23 nm, while the average height for the same strands after irradiation was 338 ± 34 nm. These results were obtained as an average of 18 cuticle step heights (eight measurements in strand 1, six measurements in strand 2 and four measurements in strand 3 (not shown)).

In all the cases, the edge heights measured by AFM lie within the typical range of cuticle heights reported in literature, which goes from 200 to 500 nm [16]. In spite of this, in our measurements at RH < 15%, the step height in photodegraded samples was systematically about 100 nm higher. The increase in the step height is probably a consequence of the partial detachment of the cuticle scales. This detachment may be assigned to the degradation of the internal cuticle layers, for example the cell membrane complex, responsible for the adhesive contact between two overlapping cuticle scales. Without this adhesive layer, the intercuticle contact is loose and the scales are more prone to lifting. Cuticle partial detachment due to irradiation was an effect also observed in FESEM images, as shown in Fig. 3 for a single-donor strand of dark brown hair after 600 h of irradiation with a mercury lamp. Many cuticle layers were moved up, as indicated by the arrows in Fig. 3, showing the possible reason for the increased edge heights measured by AFM in photodegraded samples. The cuticle lifting due to irradiation on hair surface can be responsible for macroscopically noticeable optical effects, such as shine decrease in hair shafts, due to light scattering by the irregular cuticle surface. Shine decrease and cuticle lifting in UV irradiated hair were also reported by Coderch et al. [19], who carried out FESEM and gloss measurements on standard dark brown hair from De Meo Brothers Inc., after irradiation for 36 h, with a light source simulating UV solar irradiation (500 W/m^2).

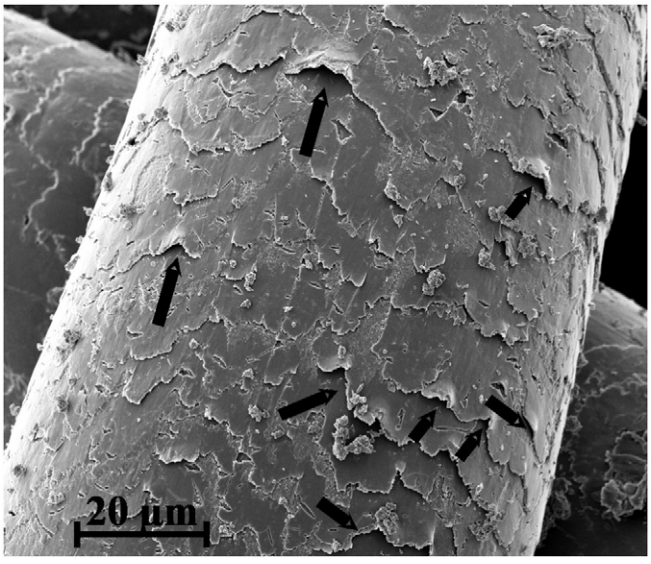

Fig. 3. FESEM images obtained on the cuticle surface of a single-donor dark brown hair after 600 h of irradiation with a mercury lamp. The arrows indicate the detachment of the cuticle layers.

Changes in hair morphology due to UV irradiation were also reported by Weigmann et al. [8,9], but the conditions used by these authors are much more severe and not comparable to the ones used in our present work. They used a solar simulator with a xenon lamp (50.6 W/m^2 in the 300–400 nm range) to irradiate blended brown hair (De Meo Brothers Inc.) for up to 700 h at alternating three-hour cycles of humidification (at RH = 95%, 40 °C) and UV irradiation (50 °C, with relative humidity decreasing from 95% to 10% within 30 min, then remaining at 10% for 2.5 h). Using FESEM, they observed a smoother topography on hair strands irradiated for 700 h and under high humidity levels (RH = 95%), due to cuticle collapse and fusion. In this case, thinning of the cuticle edges is observed and the author's hypothesis to explain this phenomenon is protein photodegradation in the surface cuticle cell forming soluble, low-molecular weight peptides, which are able to diffuse into the internal cuticle cell layers or out of the hair strands. According to the authors, this process is highly dependent on the swollen state of the sample and was observed under UV exposition at RH = 95%, but not at RH = 10% [9]. Considering the very distinct experimental conditions applied in our work (RH = 44% and 16.5 W/m^2 in the 260–400 nm range) it should not be expected that the final result on cuticle morphology would be comparable.

Amplified images obtained on the surface of one of the cuticle scales from Fig. 2 reveal interesting photodegradation features. The topography of the cuticle from a non-irradiated hair strand is characterized by a flat and at times lightly wavy surface, as shown in Fig. 4 (a). Two relatively large cracks can be observed in these images, as indicated by C, and they help to certify that the same area was scanned in all the cases. After 230 h of lamp irradiation, small bumps start to appear on the cuticle surface, as can be observed in Fig. 4 (b). The bumps became more pronounced and distinct in the topography image of the cuticle surface after 500 h of lamp irradiation (Fig. 4 (c)). The formation of bumps after mercury lamp irradiation is highlighted in Fig. 4 (d–f) and (g–i), which show AFM amplitude and phase contrast images, respectively. All the images in Fig. 4 were obtained in the same surface area. Phase and amplitude contrasts are sensitive to topography differences, but also to chemical and mechanical properties of the surface, such as stiffness and adhesion, and also to magnetic and electric potential distributions. For this reason, these two sample scanning modes can result in improved contrast of certain surface details, such as the bumps. Line profiles traced in the positions indicated by 1, 2 and 3 in Fig. 4 (a–c) show that the smoother topography observed in non-irradiated hair strands (Fig. 4 (j)) became much more uneven after irradiation (Fig. 4 (k) and (l)), due to the bump formation. This effect was confirmed by RMS roughness measurements presented in Fig. 4 (a–c). The same area (1 µm × 1 µm in size) was selected for roughness calculation in images obtained before and after irradiation. The RMS roughness was 2.3 nm before irradiation (Fig. 4 (a)) and 3.6 nm after 500 h of irradiation (Fig. 4 (c)). Longo et al. also observed roughness increase on the surface of blended dark hair samples (De Meo Inc.) irradiated by a xenon lamp for 160 h in 2 h cycles (RH = 50% for 102 min, followed by RH = 100% for 18 min). The average roughness measured in AFM images increased from 5.4 in non-irradiated samples to 16 in exposed hair strands. The small bumps at nanometer scale were not observed in this previous work, though the roughness values increased [10].

The same area on the hair strand presented in Fig. 4 was also analyzed by FESEM after a 500 h photodegradation period and is presented in Fig. 5 (b). Index C here also indicates the same cracks previously identified in Fig. 4, confirming that the same area was scanned. The bumps distributed over the whole cuticle surface can also be observed, using this different microscopy technique (FESEM). Fig. 5 (a) shows a typical surface of non-irradiated blended dark brown hair in a different sample area, showing that the bumps were not present before irradiation. It was not possible to obtain FESEM images from the same area before and after irradiation, because the FESEM sample preparation includes a metallic sputtering step, which would certainly interfere with the surface response to irradiation. AFM is a more suitable technique for this kind

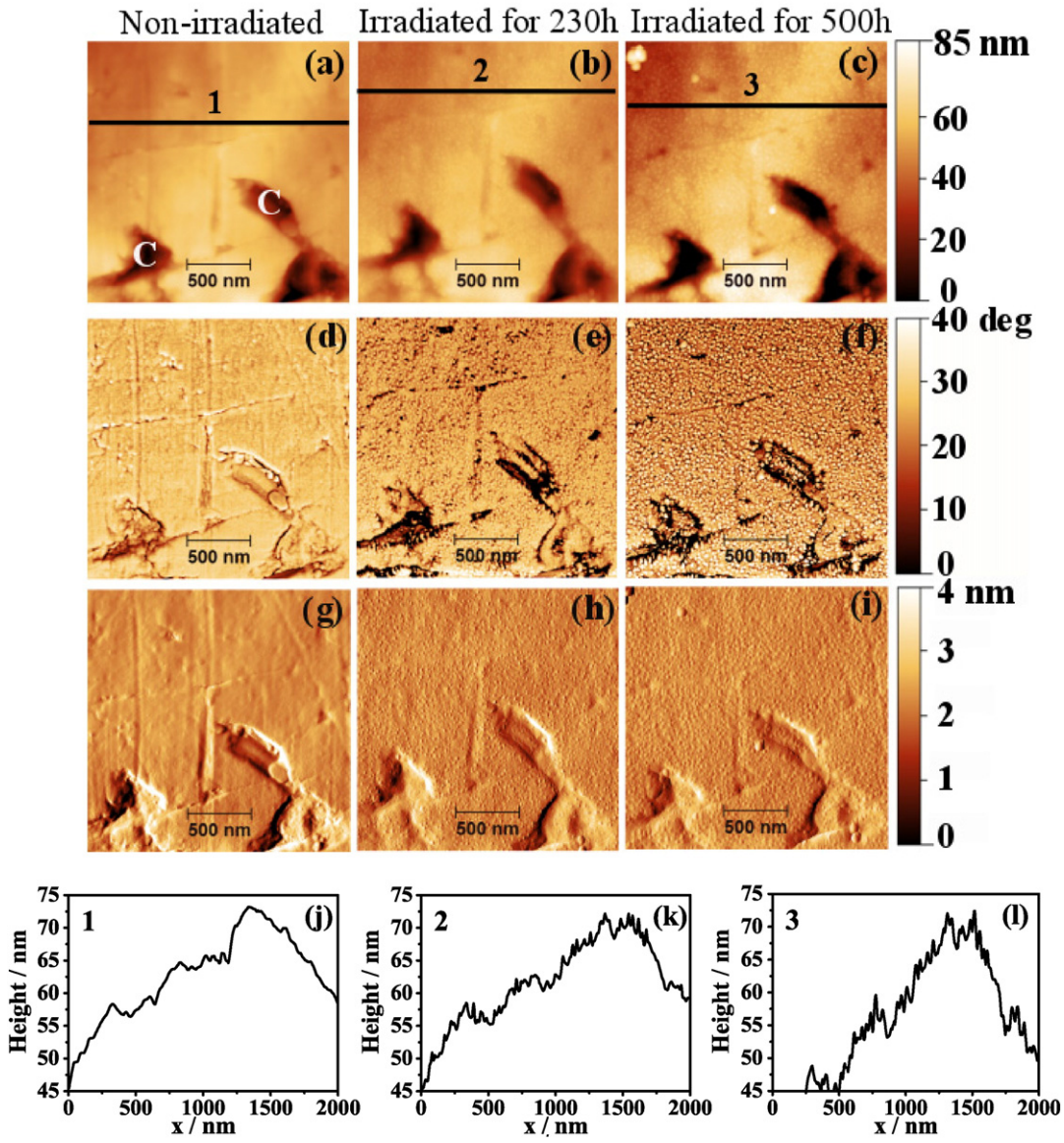

Fig. 4. AFM results from the same area of blended dark brown hair before and after irradiation with a mercury lamp: (a–c) Topography; (d–f) Amplitude; (g–i) Phase contrast images and (j–l) line profiles obtained before (j) and after irradiation for 230 h (k) and 500 h (l). Lines 1 in (a), 2 in (b) and 3 in (c) indicate the position of the line profiles shown in (j), (k) and (l), respectively. Index C (in (a)) indicates the same two cracks present in all the images.

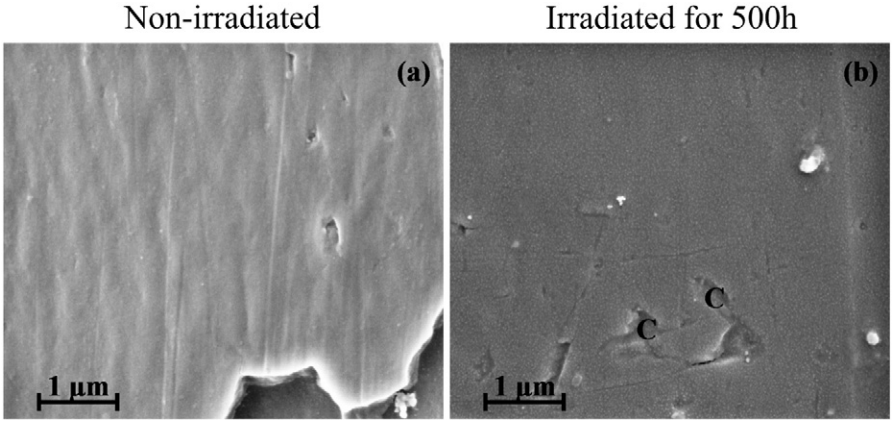

Fig. 5. FESEM images obtained on the cuticle surface of blended dark brown hair showing: (a) a typical flat surface from a non-irradiated strand; and (b) bumps formed under irradiation with a mercury lamp for 500 h. The area presented in (b) is the same previously imaged by AFM in Fig. 2, showing the same cracks (indicated by C).

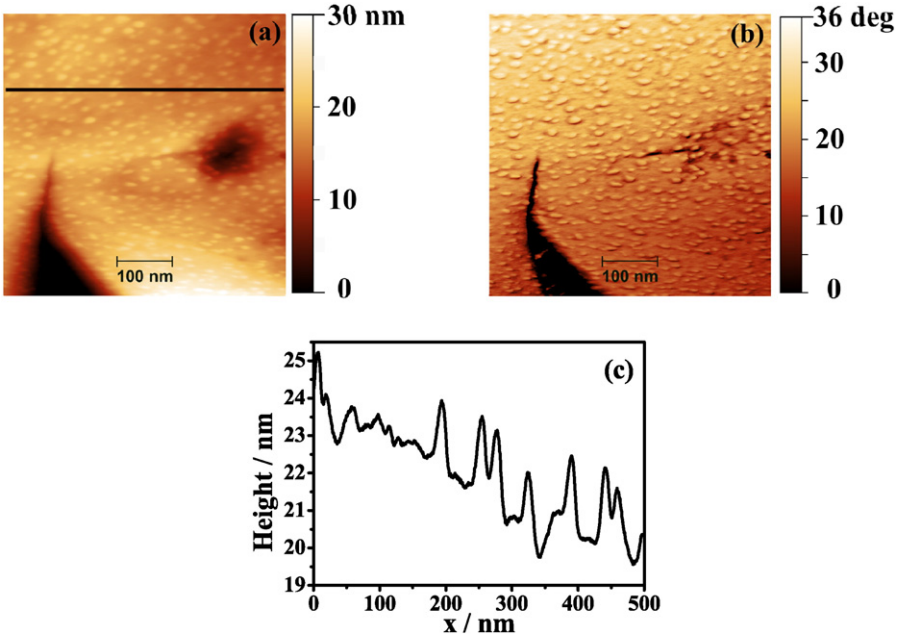

Fig. 6. AFM results obtained with a thin tip ($\phi \cong 3$ nm) from the same area of a blended dark brown hair strand exposed to a mercury lamp for 230 h: (a) topography; (b) phase contrast image and (c) line profile obtained in the black line indicated in (a). The average height of the bumps lies in the 1–5 nm range.

of observation. Nevertheless, FESEM images are useful to show that the cuticle surfaces in non-irradiated hair strands present typical flat surfaces, without bumps, as shown by the example in Fig. 5 (a). They also confirm that the bumps present in irradiated samples are distributed over the whole strand surface.

To obtain improved resolution of the bump topography, a thinner AFM tip (3 nm mean diameter) was used for sample scanning. Fig. 6 shows topography (a) and phase contrast (b) images, together with the line profile (c) from the black line indicated in (a) for dark brown hair exposed to irradiation for 230 h. The bumps present a globular shape, as shown both by the topography (Fig. 6 (a)) and the phase contrast images (Fig. 6 (b)), with heights lying in the 1 to 5 nm range (Fig. 6 (c)).

The heights of the bumps reaching 5 nm indicate that the photodegradation process must be affecting not only the lipidic layer that covers the outermost cuticle layer, but also the epicuticle layer underneath. In general, the cuticle surface is covered by a lipidic layer ($\approx$2.5 nm of thickness) that consists of 18-methyleicosanoic acid (18-MEA). The 18-MEA lipids are covalently bound to the cystine-rich layer, namely epicuticle ($\approx$10 nm of thickness), possibly

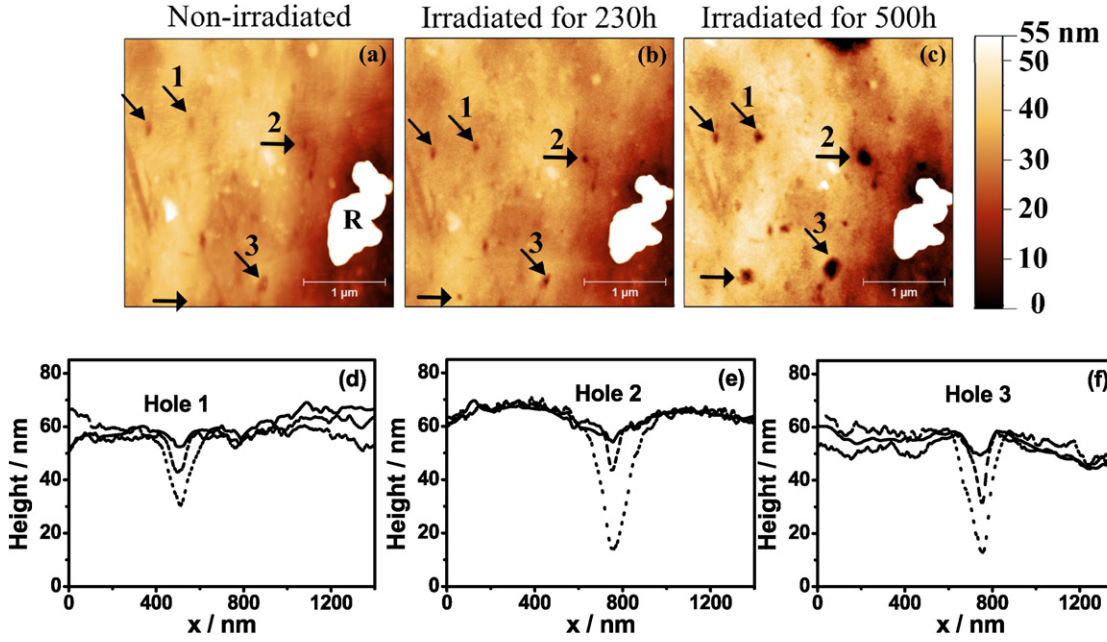

Fig. 7. AFM topography images of the same area of blended dark brown hair: (a) before and after irradiation with a mercury vapor lamp for (b) 230 h and (c) 500 h, showing the enlargement of the holes (indicated by the arrows) due to irradiation. Line profiles in (d), (e) and (f) were obtained from holes 1, 2 and 3, respectively, before (—) and after irradiation for 230 h (— — —) and 500 h (•••). Index R (in (a)) indicates the same surface defect present in all the images.

via a thioester linkage [20,21,22]. As the mean bump height measured in Fig. 6 is higher than the lipid layer, a deeper damaging effect must be taking place on the surface. It is difficulty to indicate the cause for the bump formation, since our knowledge about the chemical composition of the system is limited to the FTIR data, which points the oxidation of cystine to cysteic acid, as the main chemical change taking place in this surface. The AFM images show, however, that the bumps are not deposits of material on the surface, but protuberances formed by surface lifting. Therefore, a possible hypothesis for the formation of the bumps after irradiation is that photodegradation reactions in the internal cuticle layers may cause gas release, and this gas is trapped inside the bumps, forming small bubbles covered by a thin film of epicuticle and, possibly, part of the cuticle layers underneath.

Another photodegradation effect observed in these hair samples was the enlargement of pre-existing holes on the hair strand surface. Fig. 7 (a–b) shows AFM topography images in the same area of a cuticle scale from blended dark brown hair in variable irradiation times, where black arrows indicate holes distributed on the surface. The lighter area, marked with index R on the right side of the images is a surface defect used as a reference for sample positioning, which allows the same region to be imaged in different analyses. It is possible to observe that the holes that were already present on the sample before irradiation (Fig. 7 (a)), became larger after irradiation for 230 h (Fig. 7 (b)) and even larger after a 500 h irradiation period (Fig. 7 (c)). The pre-existing holes in Fig. 7 (a) were a 8 ± 4 nm depth with a 150 ±48 nm diameter. The mean hole diameter did not change significantly after 230 h of lamp irradiation (Fig. 7 (b)), but they became much deeper (mean depth = 14 ± 7 nm) as a consequence of the incident radiation. After a 500 h period of lamp exposure, both the diameter ($\phi = 197 \pm 50$ nm) and the depth (35 ± 12 nm) of the holes were significantly enlarged (Fig. 7 (c)). It is important to notice that both the diameter and the height measurements may be overestimated due to tip convolution, but the hole enlargement is evident from this values anyway. The line profiles presented in Fig. 7 (d–f) were obtained from holes 1, 2 and 3, indicated in Fig. 7 (a–c), and they show very clearly the increase in the hole depth as a consequence of the irradiation process. The hole enlargement after irradiation is probably caused by degradation and removal of cuticle material from the borders and from internal cuticle layers, thus deepening the cavity. It is also noticeable that the evolution of the bumps, already discussed in Figs. 4 to 6, is also observed here on the surface around the holes, in a different area of a different hair strand.

The hypothesis for the hole enlargement by removal of cuticle material is reinforced by the observation that irradiation degrades residues (of broken hair pieces probably) deposited on the strand surface. Fig. 8 shows AFM results obtained in the same area of a cuticle scale of blended brown hair. Topography images from the hair strand surface before (Fig. 8 (a)) and after irradiation for 230 h (Fig. 8 (b)) and for 500 h (Fig. 8 (c)) show that the mound (indicated by M in (a)) is partially degraded under irradiation. In the amplitude AFM images (Fig. 8 (d–f)) obtained in the same sample area and irradiation conditions, it is also possible to observe the partial degradation of the surface residues as a consequence of the irradiation. Some areas on the mound are more degraded than others, as it is possible to note comparing the regions marked by “edge” or “center” in Fig. 8 (c). The line profiles shown in Fig. 8 (g), (h) and (i) were obtained from lines 1, 2 and 3, indicated in Fig. 8 (a–c), and showed that the mound height, which was around 130 nm in the non-irradiated sample (Fig. 8 (g)), decreased to a ca. 100 nm height after irradiation for 230 h (Fig. 8 (h)) and 500 h (Fig. 8 (i)).

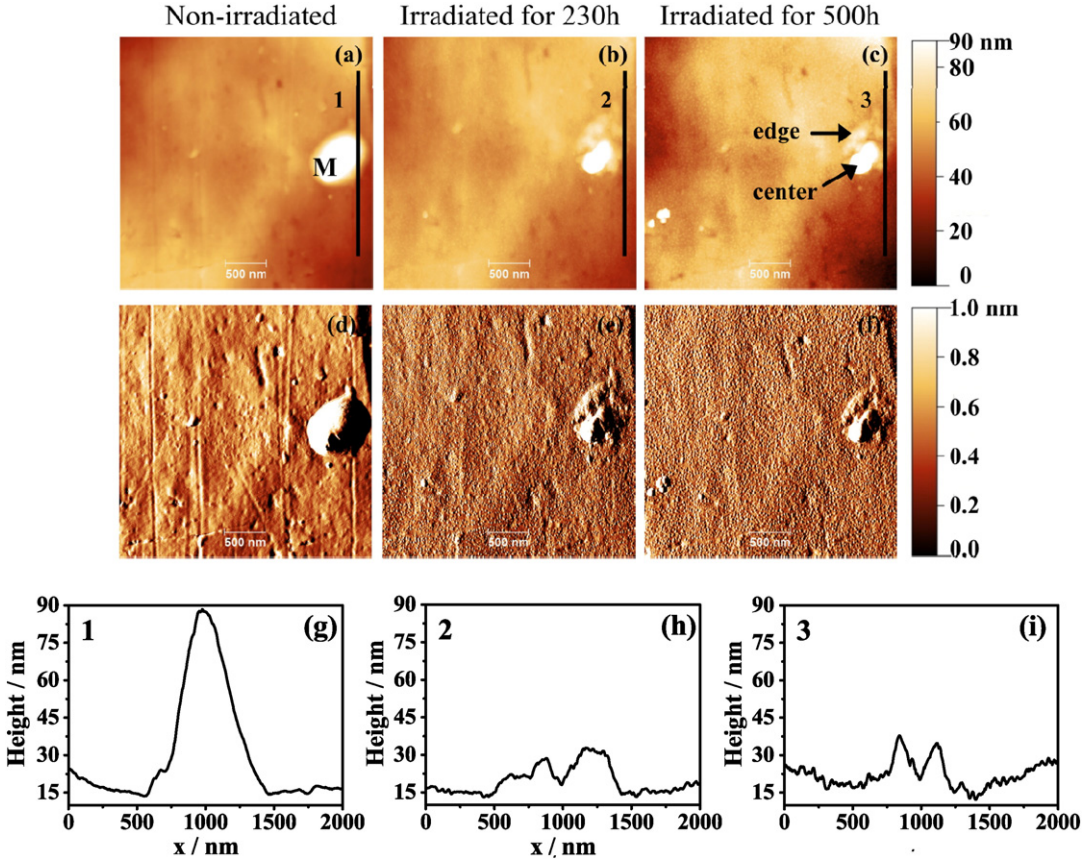

Fig. 8. AFM results from the same area of blended dark brown hair before and after irradiation with a mercury lamp: (a–c) Topography; (d–f) Amplitude images and (g–i) Line profiles obtained before (a, d, g) and after irradiation for 230 h (b, e, h) and 500 h(c, f, i). Line 1 in (a), 2 in (b) and 3 in (c) indicate the position of the line profiles showed in (g), (h) and (i), respectively. Index M in (a) indicates a mound that is partially degraded by photodegradation.

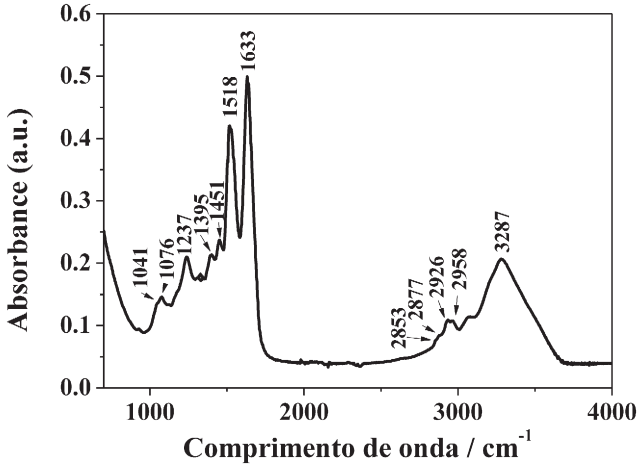

Fig. 9. ATR-FTIR spectrum of a dark brown hair strand (single-donor) before irradiation, with the characteristic hair spectral bands indicated by arrows.

3.2. Chemical Changes with Irradiation

Chemical changes in hair structure due to irradiation were investigated using the ATR-FTIR technique. Fig. 9 shows a spectrum of dark brown hair from a single-donor before irradiation, where characteristic bands from hair can be identified. The peak at 1041 cm^{-1} is due to the oxidation product (S═O) of di-sulfide bonds present in keratin. The band at 1076 cm^{-1} is assigned to C—C skeletal vibrations, while the amide III band appears at 1237 cm^{-1}. The peaks at 1395 cm^{-1} and 1451 cm^{-1} are assigned to C—H bending vibrations of CH_3 and CH_2 groups, both found in proteins and lipids. The peaks at 2853 cm^{-1} and 2926 cm^{-1} are attributed to C—H symmetric and asymmetric stretching vibrations, respectively, of CH_2 groups, and the ones at 2877 cm^{-1} and 2958 cm^{-1} refer to the same stretching modes from CH_3 groups, respectively. The two most intense peaks are assigned to amide II band: the one at 1518 cm^{-1} is mainly related to the N—H bending with some contributions from C—H stretching vibration, while the amide I band at 1633 cm^{-1} is related to C═O stretching vibrations. Finally, the peak at 3287 cm^{-1} is due to O—H stretching.

Fig. 10 shows ATR-FTIR spectra comparing two types of dark brown hair: 1. blended and 2. single-donor, before and after irradiation. To investigate the chemical changes in hair surface as a consequence of photodegradation, the bands at 1041 cm^{-1} (due to S═O stretching) and 2926 cm^{-1} (due to CH_2 stretching) were analyzed. These bands were used as indicators of changes in the cystine oxidation level (1041 cm^{-1}) and in the amount of lipids (2926 cm^{-1}) [18]. For this purpose, ATR spectra were separated in ranges from 950 to 1473 cm^{-1} (Fig. 10 (a)) and from 2800 to 3000 cm^{-1} (Fig. 10 (b)). The difference in hair spectra, obtained by subtracting the spectrum of the non-irradiated hair from the spectrum of the irradiated one, is shown in Fig. 10 (c) and (d).

The ATR-FTIR results show an increase of the cystine oxidation level with irradiation, as evidenced by the increased peak intensity at 1041 cm^{-1} (cysteic acid, —SO_3H) in the irradiated strands in Fig. 10 (a) and (c). It is well known in the literature that UV radiation converts the S—S covalent bond present in cystine into a —SO_3 group, leading to the formation of cysteic acid [23]. These results thus show a clear effect of the cystine oxidation during irradiation. Considering the quantity of lipids in the cuticle, no significant variations were observed in Fig. 10 (b) and (d) when samples before and after irradiation were compared. This result indicates that the lipids were not removed or chemically modified by photodamaging.

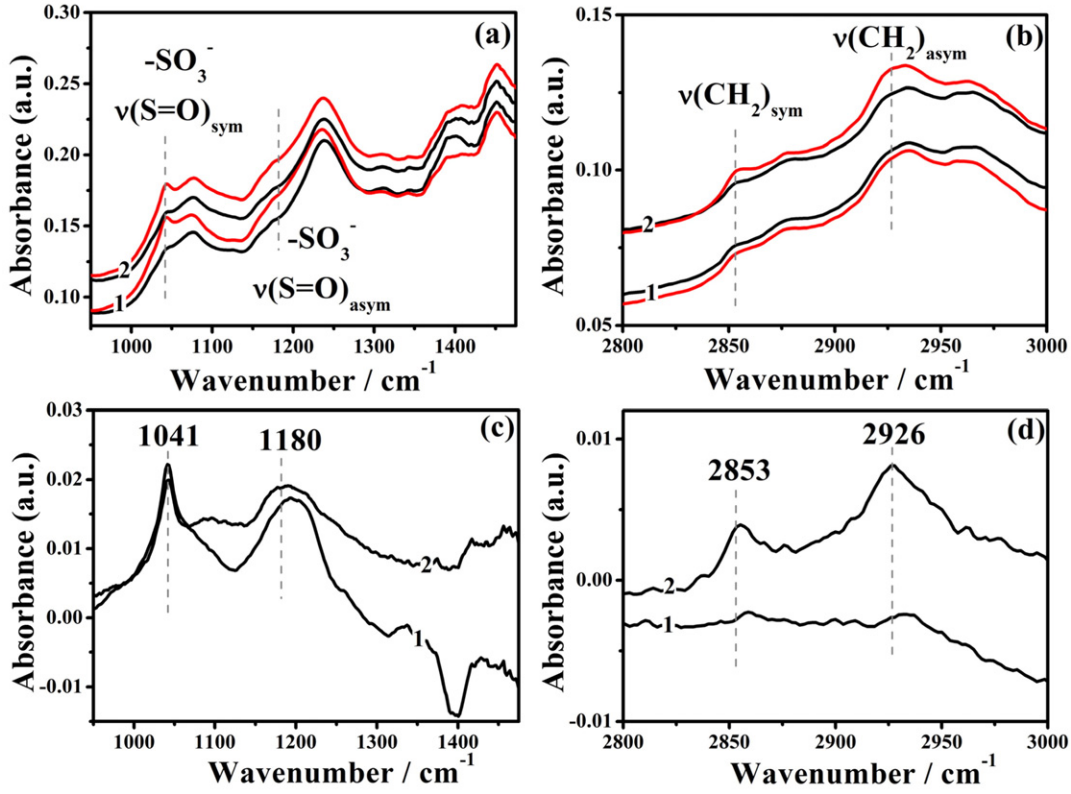

Fig. 10. (a) and (b) Non-normalized ATR-FTIR spectra of the two hair types at 950–1475 cm^{-1} and 2800–3000 cm^{-1} comparing hair before irradiation (●) and after 500 h of lamp irradiation (●). (c) and (d) Difference spectra highlighting the photodegradation effect after 500 h of lamp irradiation. Two types of hair were analyzed: 1. blended dark brown hair (line 1) and 2. Single-donor dark brown hair (line 2). The values in the spectra are averages of five different hair strands from in each sample.

Also the contact angles were measured on the hair strands to investigate the possible changes in their hydrophobic character and to obtain an indicative of the irradiation effects on the lipid layer covering the cuticle surface. Table S1 in supplementary material shows the averaged contact angle values obtained from 30 images of water droplets deposited in 10 different strands from each hair sample. The average angle values for blended hair before 74 ± 9° and after irradiation for 500 h (76 ± 7°) and for single-donor hair before (71 ± 9°) and after irradiation for 500 h (64 ± 8°) are all very similar, considering the standard deviations in both types of hair, and a significant tendency cannot be identified by comparing hair strands irradiated for 500 h and the non-irradiated hair (Table S1). It indicates that the lipid layer covering the cuticle surface do not seem to be changed or removed by irradiation to an extent that would change the surface hydrophobicity. These results are in agreement with the ATR-FTIR data.

Returning to the AFM results in the light of the contact angle measurements, we can infer that the formation of bumps up to 5 nm height reaches internal layers from cuticle cell, without changing the chemical characteristics of the 18-MEA lipid layer deposited on it or changing significantly its hydrophobic character.

4. Conclusions

The results presented herein indicate that the morphology of hair outermost cuticle is significantly modified after irradiation with a mercury lamp. The irradiation process resulted in the formation of small bumps with a globular shape (up to 5 nm height) on all hair surfaces. Likewise, enlargement of pre-existing holes, degradation of residues on the cuticle surface and an increase in the height of the steps formed between two adjacent cuticle scales were also observed as photodegradation effects. These morphological changes were followed by an increase in the cystine oxidation level, but by no apparent modification in the quantity of the lipids on the hair surface. Thus, the bump formation probably reaches internal layers from cuticle cell, without altering the chemical characteristics of its lipid covering layers.

Acknowledgments

The authors thank CAPES for financial support and also the LME/LNNano/CNPEM for the technical support during the electron and the atomic force microscopy analyses.

Appendix A. Supplementary data

Supplementary data to this article can be found online at http://dx.doi.org/10.1016/j.jphotobiol.2015.10.008.

References

[1] M. Richena, M. Silveira, C.A. Rezende, I. Joekes, Yellowing and bleaching of grey hair caused by photo and thermal degradation, J. Photochem. Photobiol. B Biol. 138 (2014) 172–181.
[2] A.C.S. Nogueira, M. Richena, L.E. Dicelio, I. Joekes, Photo yellowing of human hair, J. Photochem. Photobiol. B Biol. 88 (2007) 119–125.
[3] A.C.S. Nogueira, I. Joekes, Hair color changes and protein damage caused by ultraviolet radiation, J. Photochem. Photobiol. B Biol. 74 (2004) 109–117.
[4] E. Fernández, C. Barba, C. Alonso, M. Martí, J.L. Parra, L. Coderch, Photodamage determination of human hair, J. Photochem. Photobiol. B Biol. 106 (2012) 101–106.
[5] E. Hoting, M. Zimmermann, S. Hilterhaus-Bong, Photochemical alterations on human hair. Part I: artificial irradiation and investigations of hair proteins, J. Soc. Cosmet. Chem. 46 (1995) 85–99.
[6] E. Hoting, M. Zimmermann, H. Hocker, Photochemical alterations on human hair. Part II: analysis of melanin, J. Soc. Cosmet. Chem. 46 (1995) 181–190.
[7] E. Hoting, M. Zimmermann, Photochemical alterations in human hair. Part III. Investigations of internal lipids, J. Soc. Cosmet. Chem. 47 (1995) 201–211.
[8] S.B. Ruetsch, Y. Kamath, H.D. Wegmann, Photodegradation of human hair: an SEM study, J. Cosmet. Sci. 51 (2000) 103–125.
[9] S.B. Ruetsch, Y. Kamath, H.D. Wegmann, Photodegradation of human hair: a microscopy study, in comprehensive series in photosciences, sun protection in man, 3Elsevier Science, 2001 175–205 Chapter 9.
[10] V.F. Monteiro, A.S. Pinheiro, E.R. Leite, J.A.M. Agnelli, M.A. Pereira-da-Silva, E. Longo, UV radiation: aggressive agent to the hair — AFM, a new methodology of evaluation, J. Cosmet. Sci. 54 (2003) 271–281.
[11] W.T. Astbury, A. Street, X-Ray studies of the structure of hair, wool, and related fibres. I, General. Philosophical Transactions A, 230 1932, pp. 75–101.
[12] J.A. Swift, A.W. Holmes, Degradation of human hair by papain. Part III. Some electron microscope observations, Text. Res. J. 35 (1965) 1014–1019.
[13] J. Lindberg, B. Philip, N. Gralén, Occurrence of thin membranes in the structure of wool, Nature 162 (1948) 458–459.
[14] C. Dubief, Experiments with hair photodegradation, Cosmet. Toiletr. 95 (1992) 107.
[15] C.R. Robbins, Chemical aspects of bleaching human hair, J. Soc. Cosmet. Chem. 23 (1971) 339–348.
[16] J.A. Swift, J.R. Smith, Atomic force microscopy of human hair, Scanning 2 (2000) 310–318.
[17] S. Breakspear, J.R. Smith, Returning to the same area of hair surfaces before and after treatment: a longitudinal AFM technique, J. Microsc. 215 (2004) 34–39.
[18] M. Korte, S. Akari, H. Kuhn, N. Baghdadli, H. Mohwald, G.S. Luengo, Distribution and localization of hydrophobic and ionic chemical groups at the surface of bleached human hair fibers, Langmuir 41 (2014) 12124–12129.
[19] E. Fernández, B. Martínez-Teipel, R. Armengol, C. Barba, L. Coderch, Efficacy of antioxidants in human hair, J. Photochem. Photobiol. B Biol. 117 (2012) 146–156.
[20] D.W. Cheong, F.C.H. Lim, L. Zhang, Insights into the structure of covalently bound fatty acid monolayers on a simplified model of the hair epicuticle from molecular dynamics simulations, Langmuir 28 (2012) 13008–13017.
[21] J.R. Smith, Use of atomic force microscopy for high-resolution non-invasive structural studies of human hair, J. Soc. Cosmet. Chem. 48 (1997) 199–208.
[22] C.R. Robbins, The cell membrane complex: three related but different cellular cohesion components of mammalian hair fibers, J. Cosmet. Sci. 60 (2009) 437–465.
[23] C.R. Robbins, M.J. Bahl, Analysis of hair by electron spectroscopy for chemical analysis, J. Soc. Cosmet. Chem. 35 (1984) 379–390.